IOP Publishing Journal of Physics: Condensed Matter

J. Phys.: Condens. Matter **32** (2020) 195801 (7pp) https://doi.org/10.1088/1361-648X/ab6e8f

Scaling of the magnetic entropy change in chiral helimagnetic $YbNi_3Al_9$

Yamei Wang[1,2], Wei Liu[1,2], Jun Zhao[1,2], Fanying Meng[1,2], Jiyu Fan[3], Min Ge[4], Li Pi[1,4], Lei Zhang[1,5] and Yuheng Zhang[1,4]

[1] Anhui Key Laboratory of Condensed Matter Physics at Extreme Conditions, High Magnetic Field Laboratory, Chinese Academy of Sciences, Hefei 230031, People's Republic of China
[2] University of Science and Technology of China, Hefei 230026, People's Republic of China
[3] Department of Applied Physics, Nanjing University of Aeronautics and Astronautics, Nanjing 210016, People's Republic of China
[4] Hefei National Laboratory for Physical Sciences at the Microscale, University of Science and Technology of China, Hefei 230026, People's Republic of China

E-mail: zhanglei@hmfl.ac.cn

Received 20 October 2019, revised 20 December 2019
Accepted for publication 22 January 2020
Published 13 February 2020

Abstract

Generally, magnetic anisotropy is a common feature of a layered magnetic material, the exploration of which plays a key role in understanding the intrinsic magnetic couplings. In this work, we have studied the field-induced magnetic transitions for layered $YbNi_3Al_9$ as the external magnetic field is applied perpendicularly ($H \perp c$) and parallel ($H//c$) to the c-axis. We find that two independent universal curves of magnetic entropy change [$\Delta S_M(T, H)$] can be fitted out for $H \perp c$ and $H//c$, respectively. According to the universality principle of scaling, the extra magnetic entropy changes ($|\Delta S_M^{ab}|$ and $|\Delta S_M^{c}|$) caused by the field-induced magnetic phase transitions can be obtained for $H \perp c$ and $H//c$. The two-dimensional $|\Delta S_M^{ab,c}(T, H)|$ plots as functions of field and temperature are constructed, which clearly reveal the evolutions of the magnetic entropy changes resulted from the two different field-induced magnetic phase transitions. It is suggested that the $|\Delta S_M^{ab}(T, H)|$ for $H \perp c$ with the maximum at (3.2 K, 4.1 kOe) originates from a field-modulated helicoidal spin-texture. However, the $|\Delta S_M^{c}(T, H)|$ for $H//c$ with the maximum at (3.4 K, 13.8 kOe) stems from a field-induced canted antiferromagnetic state.

Keywords: two-dimensional layered material, magnetic entropy change, scaling, field-induced magnetic transition, chiral helimagnetism

(Some figures may appear in colour only in the online journal)

1. Introduction

Recently, isolated chiral magnetic states such as magnetic skyrmion have triggered great interest due to their potential applications in spintronic devices [1–9]. These isolated chiral magnetic states can form chiral magnetic phases, such as as magnetic skyrmion lattice [9]. When tuned by external magnetic or electric field, these isolated spiral spin-textures can be generally treated as stable particle-like object with special features involving topological protection, nano-metric size, and easily current-driven motion [8–10]. Particularly, in uniaxial ferromagnetic material, a one-dimensionally modulated spiral state at low fields and a new vortex state in an intermediate field range can emerge due to the competition between the Dzyaloshinskii–Moriya (DM) interaction and ferromagnetic exchange [11–13]. Among these exotic chiral spin-textures, a helicoidal spin-texture has been predicted theoretically [14]. Under external magnetic field, this helicoidal structure is modulated into magnetic superlattice consisting of magnetic kinks with a ferromagnetic background. This magnetic superstructure of helicoid has been verified experimentally in uniaxial noncenrosymmeric ferromagnet $YbNi_3Al_9$ as well as the Cu-doped $Yb(Ni_{1-x}Cu_x)_3Al_9$, which belongs to the crystallographic class C_{3v} [15–18].

[5] Author to whom any correspondence should be addressed.

 © 2020 IOP Publishing Ltd Printed in the UK

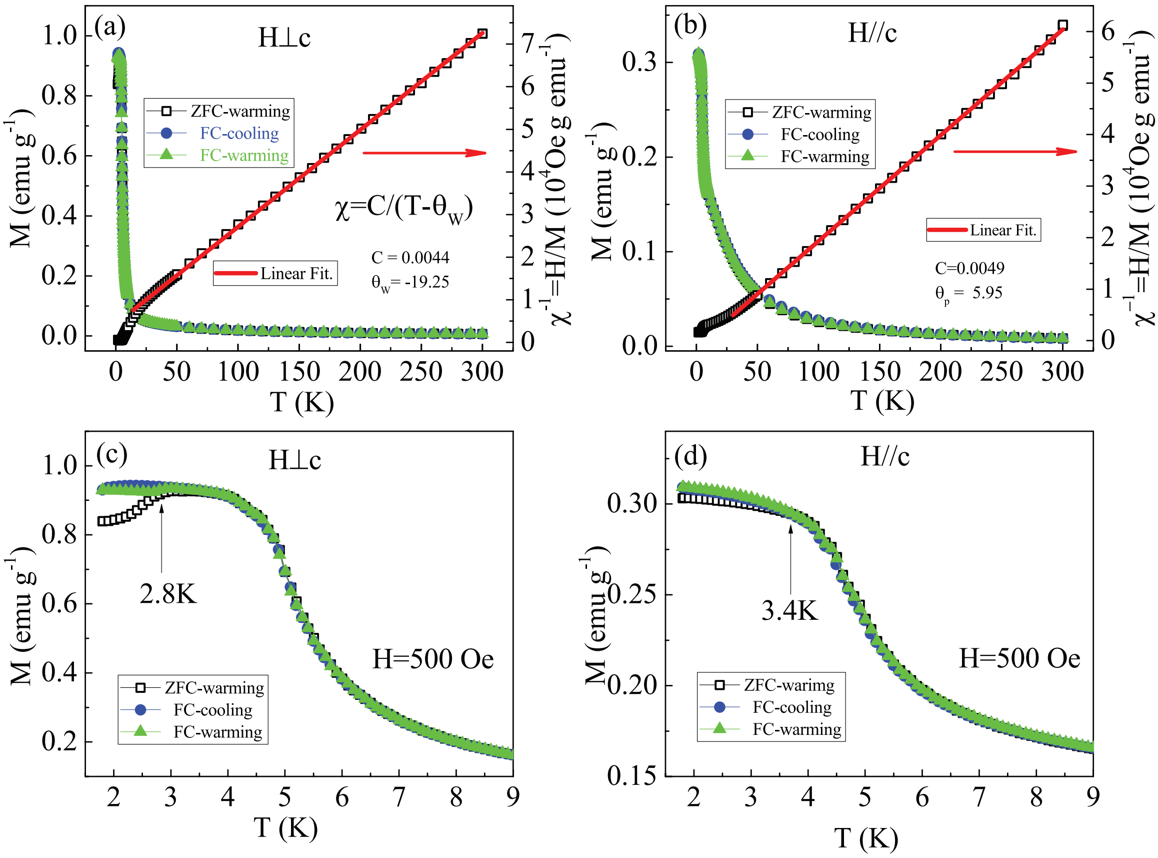

Figure 1. (a) and (b) Temperature dependence of magnetization [$M(T)$] (left-axis) and reciprocal susceptibility [$\chi^{-1}(T)$] (right-axis) with $H \perp c$ and $H//c$ respectively; (c) and (d) the magnified $M(T)$ curves at low temperature.

The trigonal layered $YbNi_3Al_9$ exhibits complex magnetism [19–21]. The spiral spin-texture and magnetism in $YbNi_3Al_9$ stem from the 4*f*-electrons of trivalent Yb ions [22]. When external magnetic filed is applied perpendicularly to the *c*-axis ($H \perp c$), a magnetic superstructure of helicoid with periodicity of $L_0 = 3.4$ nm appears below $T_C \sim 3.4$ K [17]. In the Cu-doped $Yb(Ni_{1-x}Cu_x)_3Al_9$ ($x = 0.06$), $L_0 = 6.1$ nm is determined with higher $T_C \sim 6.4$ K [18]. Meanwhile, due to the anisotropic hybridization between *f*-electrons and conductive electrons, $YbNi_3Al_9$ exhibits other fascinating phenomena such as heavy fermion antiferromagnetic behavior and Kondo lattice effect [21–25]. Under hydrostatic pressure, the antiferromagnetic phase transition is suppressed and the localized character of Yb^{3+} state becomes stronger inferred from the reduction of the Kondo scattering [26].

In addition to the field-modulated helicoidal structure for $H \perp c$, $YbNi_3Al_9$ displays another field-induced magnetic transition when the external field applied parallel to the *c*-axis ($H//c$) [16]. However, the detailed mechanisms of the field-induced magnetic transitions in this system remain unclear, especially that with $H//c$. Moreover, a comparative study of field-induced magnetic transitions for $H \perp c$ and $H//c$ is also important to uncover the anisotropic characteristics in this system. In this work, we investigate the magnetic entropy changes [$\Delta S_M(T,H)$] of $YbNi_3Al_9$ for $H \perp c$ and $H//c$ by the scaling method. According to the universality principal of scaling, the extra magnetic entropy changes $|\Delta S_M^{ab}|$ and $|\Delta S_M^{c}|$ caused by the field-induced magnetic phase transitions are obtained for $H \perp c$ and $H//c$. Based on the two-dimensional (2D) $|\Delta S_M^{ab,c}(T,H)|$ plots as functions of field and temperature, the evolutions of magnetic entropy changes caused by the two different field-induced magnetic phase transitions are clearly revealed for $H \perp c$ and $H//c$.

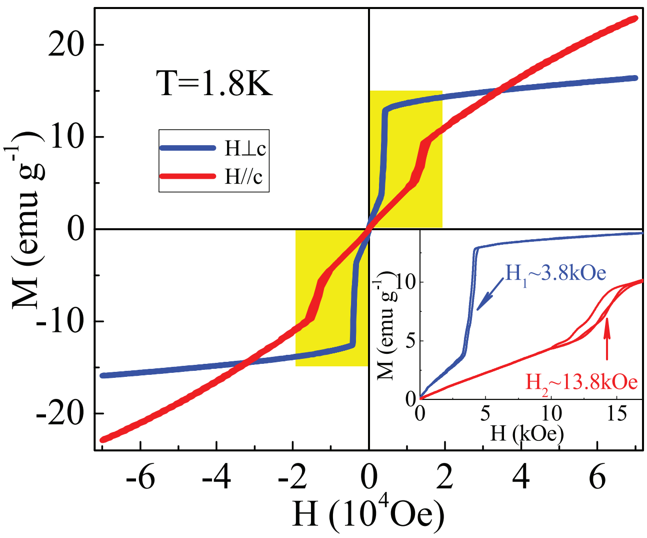

Figure 2. Field dependence of isothermal magnetization [$M(H)$] at $T = 1.8$ K with $H \perp c$ and $H//c$ (inset shows the magnified $M(H)$ in lower field (LF) region).

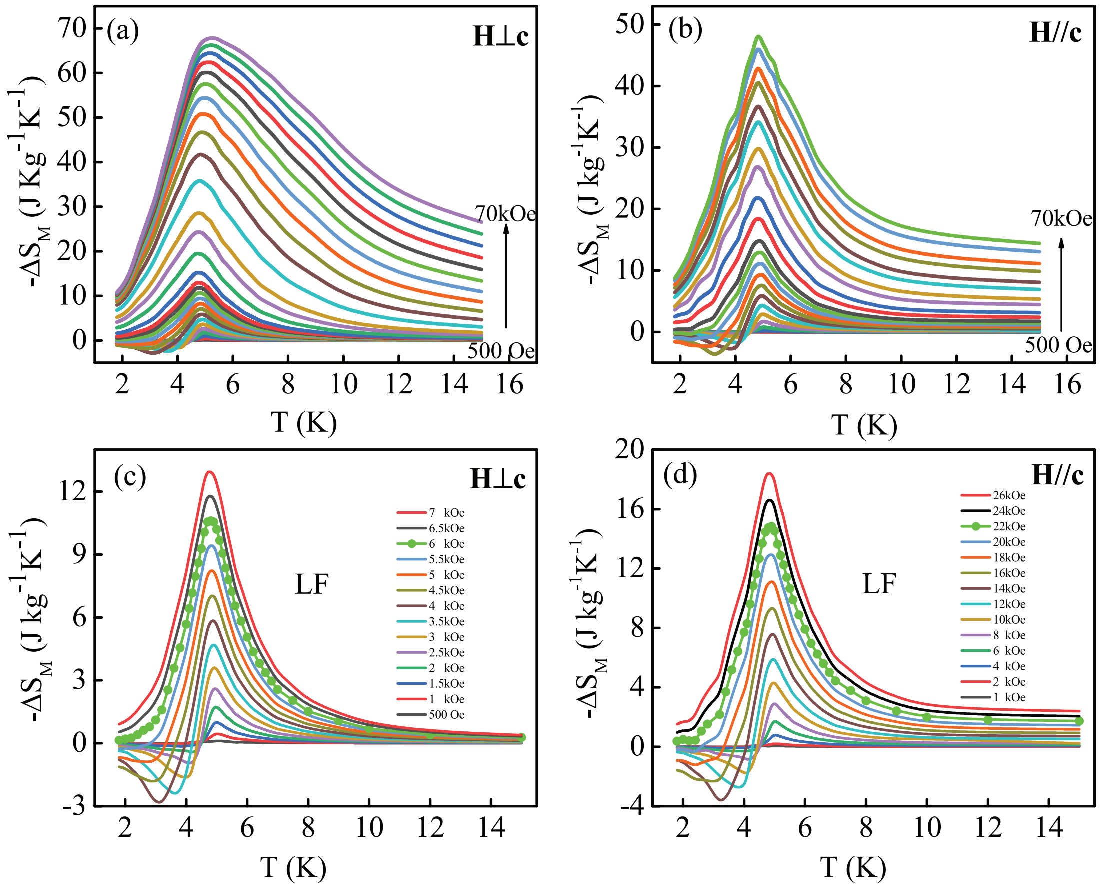

Figure 3. (a) and (b) Temperature dependence of magnetic entropy change $[-\Delta S_M(T)]$ under selected fields with $H \perp c$ and $H//c$; (c) and (d) $-\Delta S_M(T)$ curves in LF region with $H \perp c$ and $H//c$.

2. Experimental methods

Single-crystals of $YbNi_3Al_9$ were synthesized by the self-flux method. Powders of Yb (purity 3*N*), Ni (4*N*), and Al (5*N*) with a ratio of Yb: Ni: Al = 1: 3: 20 were sealed in a vacuumed quartz tube, where the extra Al was used as a flux. The mixed powder in the vacuumed tube was heated to 1173 K, and hold at that temperature for 12 h. Then, the temperature was cooled to 973 K at a rate of 2 K h^{-1}. The flux was removed by centrifugation at 973 K. Finally, the as-grown single crystals were soaked in hydrochloric acid to exclude extra flux. The chemical constituents of the single crystal were checked by energy dispersive x-ray (EDX) spectrometry, which are close to the desired proportions. The crystal structure and orientation were determined by x-ray diffraction (XRD). The magnetization was performed using a Quantum Design vibrating sample magnetometer (SQUID-VSM). The initial isothermal magnetization was carried out after the sample heated adequately above T_C with a no-overshoot mode.

3. Results and discussion

Figures 1(a) and (b) show the temperature dependence of magnetization $[M(T)]$ for $YbNi_3Al_9$ with the field applied perpendicularly ($H \perp c$) and parallel ($H//c$) to the *c*-axis, respectively. The $M(T)$ curves are measured under three sequences: measured on warming after zero-field-cooling (ZFC-warming), measured on cooling under field (FC-cooling), and measured on warming under field (FC-warming). The $M(T)$ curves in figures 1(a) and (b) display paramagnetic behaviors in higher temperature region. The right-coordinates of figures 1(a) and (b) plot the temperature dependence of reciprocal susceptibility $[\chi^{-1}(T)]$, which present linear behaviors in higher temperature region. The $\chi^{-1}(T)$ can be fitted by the Curie–Weiss law $[\chi = C/(T - \theta_W)]$, the fitting results of which are depicted as red lines in figures 1(a) and (b) (C is the Curie constant and θ_W is the Curie–Weiss temperature). Figures 1(c) and (d) display the magnified $M(T)$ curves at low temperature, which manifest that magnetic transitions occur to $YbNi_3Al_9$ for both $H \perp c$ and $H//c$. For $H \perp c$ in figure 1(c), the FC-cooling and FC-warming $M(T)$ curves overlap with each other, both of which are separated from the ZFC-warming one. However, for $H//c$ in figure 1(d), the three $M(T)$ curves under ZFC-warming, FC-cooling, and FC-warming are almost coincident. Moreover, the magnetic phase transition occurs at different temperatures for $H \perp c$ and $H//c$, where it is determined from the points of bifurcation that $T_C \sim 2.8$ K for $H \perp c$ and $T_C \sim 3.4$ K for $H//c$. In fact, the

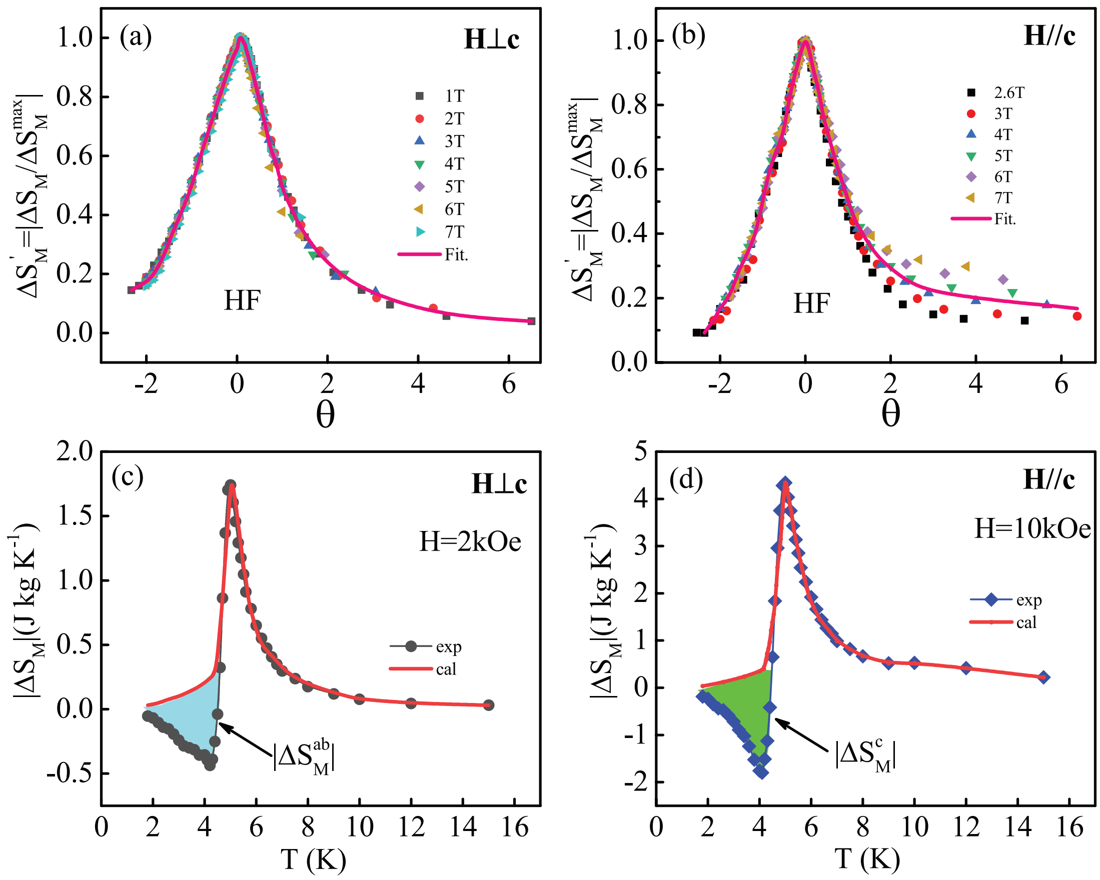

Figure 4. (a) and (b) Scaled $\Delta S'_M(\theta)$ curves in high field (HF) region with $H \perp c$ and $H//c$; (c) and (d) comparison of the experimental $|\Delta S_M(T)|$ and the calculated one for $H \perp c$ and $H//c$ in LF region.

phase transitions for $H \perp c$ and $H//c$ are absolutely different [16, 22]. For $H \perp c$, the magnetic transition originates from chiral helimagnetic ordering to paramagnetic one [17, 18]. However, the mechanism of the field induced transition for $H//c$ remains open.

Figure 2 gives the field-dependent isothermal magnetization [$M(H)$] for $YbNi_3Al_9$ at $T = 1.8$ K with $H \perp c$ and $H//c$, where the inset shows the magnified $M(H)$ curves in LF region. The $M(H)$ curves with $H \perp c$ and $H//c$ exhibit absolutely different behaviors, which are in agreement with the previous report [22]. The $M(H)$ curve with $H \perp c$ exhibits a saturated behavior, while that with $H//c$ displays an unsaturated tendency. A field-induced magnetic transition occurs to $M(H)$ curve for $H \perp c$ at ~3.8 kOe with a small hysteresis, which is a typical indication of a field-modulated helicoidal spin-texture [27]. Meanwhile, a loop occurs on $M(H)$ curve with $H//c$ at ~13.8 kOe. The different performances between $H \perp c$ and $H//c$ suggest that the field induces absolutely different magnetizing behaviors depending on the applied orientations [23]. The loop on $M(H)$ curve for $H//c$ may be caused by the destruction of the ground state. The unsaturated behavior suggests the state in higher field region should be canted-antiferromagnetic ordering [28].

As is known, the magnetic entropy change, which occurs simultaneously at the magnetic transition, is an effective method to investigate the phase transition, especially in chiral magnetic helimagnetic systems [29–32]. Generally, the magnetic entropy change $\Delta S_M(T, H)$ is expressed as [33]:

$$\Delta S_M(T,H) = \Delta S_M(T,H) - \Delta S_M(T,0) = \int_0^{H^{\max}} [\partial S(T,H)/\partial H]_T \mathrm{d}H, \quad (1)$$

with the Maxwell's relation $[\partial S(T,H)/\partial H]_T = [\partial M(T,H)/\partial T]_H$, $\Delta S_M(T,H)$ is re-written as:

$$\Delta S_M(T,H) = \int_0^{H^{\max}} [\partial M(T,H)/\partial T]_H \mathrm{d}H. \quad (2)$$

Figures 3(a) and (b) plot the temperature dependence of $-\Delta S_M$ [$-\Delta S_M(T)$] under selected field for $H \perp c$ and $H//c$, respectively. Each $-\Delta S_M(T)$ curve displays a peak at T_C. Figures 3(c) and (d) magnify the $-\Delta S_M(T)$ curves under LF. For the curve in LF region, a dip appears on each $-\Delta S_M(T)$ curve below T_C. For $H \perp c$ in figure 3(c), the dip disappears when H exceeds 6 kOe. However, for $H//c$ in figure 3(d), the dip disappears when H exceeds 22 kOe. The peak of $-\Delta S_M(T)$ is corresponding to the paramagnetic transition. The dip on $-\Delta S_M(T)$ curve is caused by the field-induced magnetic transition rather than the paramagnetic transition.

The universality principal is a guided law for the phase transition. According to the universality principal, $\Delta S_M(T, H)$ under different field can be scaled into a single universal curve, which is independent of the external field [35]. Based on the

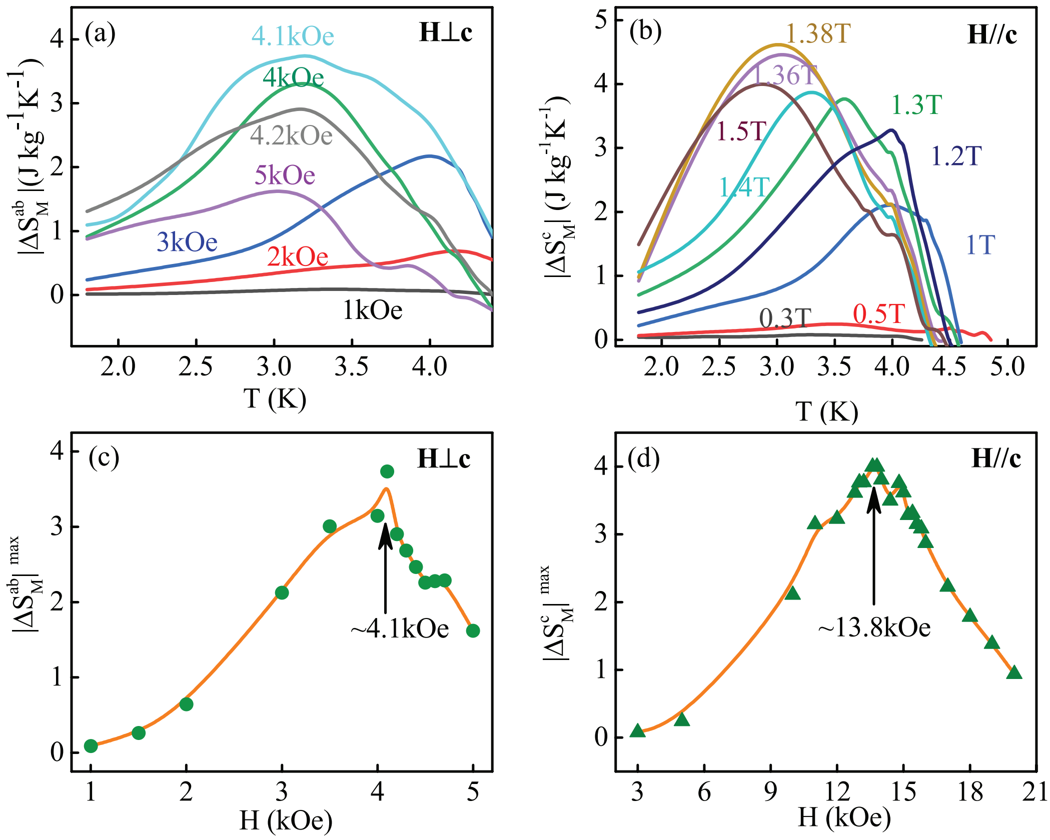

Figure 5. (a) and (b) Temperature-dependent $|\Delta S_M^{ab}|$ and $|\Delta S_M^{c}|$ of phase transitions for $H \perp c$ and $H//c$ respectively; (c) and (d) field-dependent maximum of $|\Delta S_M^{ab}|$ and $|\Delta S_M^{c}|$ for $H \perp c$ and $H//c$.

phenomenological universal scaling method, $\Delta S_M(T, H)$ is normalized as $\Delta S'_M = |\Delta S_M / \Delta S_M^{\max}|$ [34–36]. Meanwhile, the horizontal coordinate is re-scaled into a re-scaled temperature θ, which is defined as [36]:

$$\theta = \frac{T - T_C}{T_r - T_C}, \tag{3}$$

where T_r is the reference temperature. After scaling and normalizing, the universal curve would be to impose the position of T_r at a value of $\theta = 1$. However, due to the asymmetries of $\Delta S_M(T, H)$ below and above T_C, the re-scaled temperature is usually treated separately below and above T_C. Consequently, the re-scaled temperature is defined as [36]:

$$\theta = \begin{cases} \theta_- = (T_C - T)/(T_{r1} - T_C), T \leqslant T_C \\ \theta_+ = (T - T_C)/(T_{r2} - T_C), T > T_C \end{cases}, \tag{4}$$

where T_{r1} and T_{r2} are the reference temperatures below and above T_C respectively. Here, T_{r1} and T_{r2} are defined as temperatures when $\Delta S_M(T_{r1}, T_{r2}) = \frac{1}{2}\Delta S_M^{\max}$, which correspond to $\theta = -1$ (below T_C) and $\theta = +1$ (above T_C) after normalization. Based on this method, the $\Delta S_M(T, H)$ are re-scaled into $\Delta S'_M(\theta)$ curves, which should collapse into a single independent universal curve. Subsequently, an universality curve can be fitted out, which should be independent of the external field. Figures 4(a) and (b) plot the $\Delta S'_M(\theta)$ curves in higher field region for $H \perp c$ and $H//c$, respectively. The $\Delta S'_M(\theta)$ curves for $H \perp c$ in figure 4(a) collapse into a single curve, where the universal $\Delta S'_M(\theta)$ is fitted out and denoted as red curve. Similarly, $\Delta S'_M(\theta)$ curves for $H//c$ in figure 4(b) collapse into another single curve, where the universal $\Delta S'_M(\theta)$ is also fitted out. The universal $\Delta S'_M(\theta)$ is independent of the external field. Based on the universal $\Delta S'_M(\theta)$, $\Delta S_M(T, H)$ at different temperature and under different field can be calculated [37].

If a field-induced magnetic transition occurs, an extra magnetic entropy change is brought in, which can not be included in the universal scaling. Due to the suppression of the field-induced magnetic transition under higher field, the universal curves under HF do not contain these extra magnetic entropy changes which only occur under LF. The universal $\Delta S'_M(\theta)$ fitted out can be extrapolated to LF region. The discrepancy between the experimental and the calculated curves is just caused by the extra magnetic entropy change caused by the field-induced magnetic transition [38]. By this method, the extra magnetic entropy change caused by the field-induced magnetic transition can be separated from the total magnetic entropy change. Thus, the universal $\Delta S'_M(\theta)$ is extrapolated to LF region, as shown in figures 4(c) and (d). Figure 4(c) gives the experimental and calculated $|\Delta S_M|$ versus T for $H \perp c$ under typical field of 2 kOe. An extra area appears from 2 K to 5 K marked as $|\Delta S_M^{ab}|$, which is resulted from the field-induced magnetic transition for $H \perp c$. Figure 4(d) depicts the experimental and calculated $|\Delta S_M|$ versus T for $H//c$ under typical field of 10 kOe. Analogously, an extra area emerges from 2 K

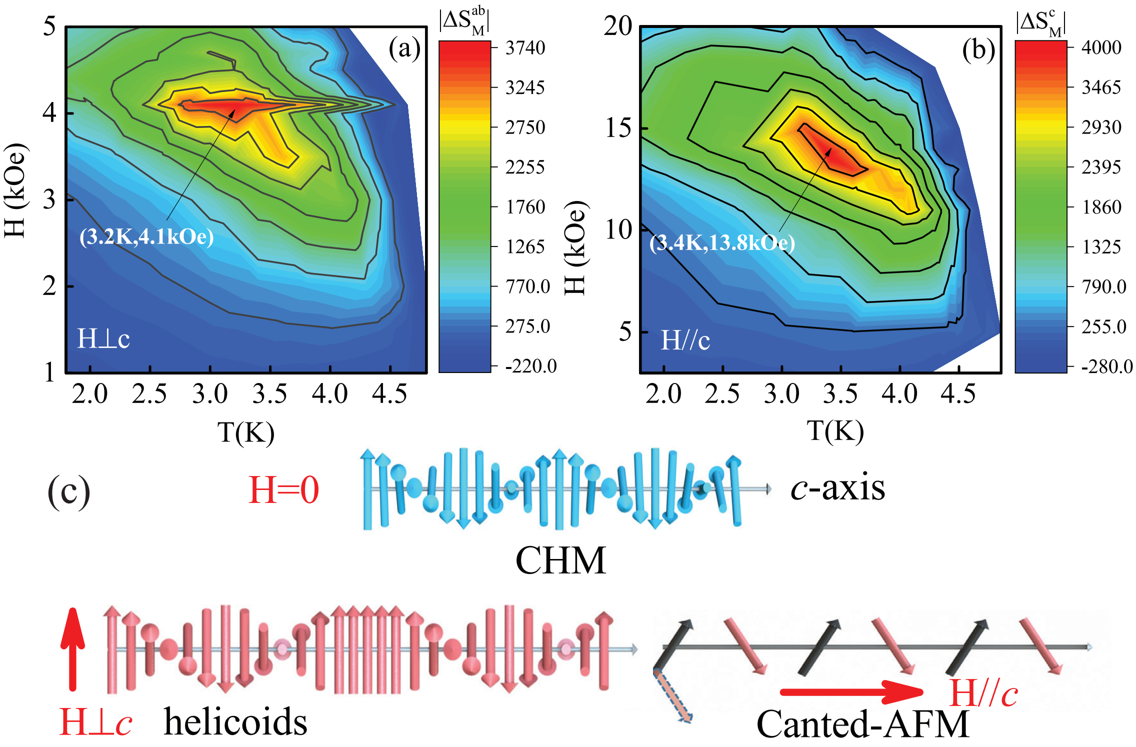

Figure 6. (a) and (b) Two-dimensional $|\Delta S_M^{ab}(T,H)|$ and $|\Delta S_M^{c}(T,H)|$ of the field-induced magnetic phase transitions for $H \perp c$ and $H//c$ respectively (red color denotes the high change while blue represents the lower one); (c) the magnetic configurations under different fields (CHM denotes chiral magnetic state, and canted-AFM is on behalf of canted-antiferromagnetic state).

to 5 K marked as $|\Delta S_M^{c}|$, which originates from the other field-induced magnetic transition for $H//c$.

By this way, the extra magnetic entropy change can be obtained by the substraction of the calculated curve from the experimental one [38]. Consequently, $|\Delta S_M^{ab,c}(T)|$ is generated as:

$$|\Delta S_M^{ab,c}(T)| = |\Delta S_M^{\exp}(T) - \Delta S_M^{\mathrm{cal}}(T)|. \tag{5}$$

Based on equation (5), the extra magnetic entropy changes caused by the field-induced magnetic transitions are calculated. Figures 5(a) and (b) depict the temperature-dependent $|\Delta S_M^{ab}|$ and $|\Delta S_M^{c}|$ of phase transitions for $H \perp c$ and $H//c$, respectively. The maximum of $|\Delta S_M^{ab}|$ and $|\Delta S_M^{c}|$ are corresponding to the greatest point of magnetic entropy change. In order to deliver clear clarification, the field-dependent maximum of $|\Delta S_M^{ab}|$ with $H \perp c$ and $|\Delta S_M^{c}|$ with $H//c$ are shown in figures 5(c) and (d). It can be seen that the magnetic entropy change reaches the maximum at ~4.1 kOe for $H \perp c$ (figure 5(a)) and ~13.8 kOe for $H//c$ (figure 5(b)).

The magnetic entropy changes caused by the field-induced magnetic phase transitions are summarized in figure 6. Figures 6(a) and (b) show the 2D $|\Delta S_M^{ab,c}(T,H)|$ plots of the phase transitions for $H \perp c$ and $H//c$ respectively, where red color denotes the high change while blue represents the lower one. From figure 6, the evolution of the magnetic entropy changes induced by the field are clearly revealed, which only occur in specific windows of field and temperature. It is known that $YbNi_3Al_9$ exhibits a chiral helimagnetic ground state (CHM) when $H = 0$ [18], as illustrated in figure 6(c). For $H \perp c$, a field-modulated helicoidal spin-texture can be induced by the external field below T_C (as shown in bottom left of figure 6(c)), to which the $|\Delta S_M^{ab}|$ is attributed. The maximum of $|\Delta S_M^{ab}(T,H)|$ is located approximately at (3.2 K, 4.1 kOe). It should be mentioned that the maximum of the magnetic entropy changes is corresponding to occurrence of the magnetic phase transition. Thus, the maximum of $|\Delta S_M^{ab}(T,H)|$ for $H \perp c$ indicates that the helicoidal spin-texture is polarized into forced ferromagnetic state at this point. For $H//c$, the maximum of $|\Delta S_M^{c}(T,H)|$ is located approximately at (3.4 K, 13.8 kOe), which indicates that the ground state is destroyed at this point. In consideration of the unsaturated behavior of $M(H)$ with $H//c$, it is concluded that a canted antiferromagnetic ordering appears after destruction of the ground state (as depicted in bottom right of figure 6(c)). Moreover, this canted antiferromagnetic ordering causes a small net magnetic moment, which increases as the field increases. However, this net magnetic moment does not reach a saturated state, which results in the unsaturated $M(H)$ behavior for $H//c$.

4. Conclusion

In summary, the magnetic entropy changes of $YbNi_3Al_9$ for $H \perp c$ and $H//c$ are systematically investigated by the scaling method. Two different kinds of magnetic transitions are induced by the external field when $H \perp c$ and $H//c$. According to the universality principle of scaling, the extra magnetic entropy change caused by the field-induced magnetic transitions are obtained, respectively. 2D $|\Delta S_M^{ab,c}(T,H)|$ plots as functions of field and temperature are constructed, which clearly uncover evolutions of the magnetic entropy change resulted from the two different field-induced magnetic phase transitions. The $|\Delta S_M^{ab}(T,H)|$ for $H \perp c$ reaches the maximum at (3.2 K, 4.1 kOe), while $|\Delta S_M^{c}(T,H)|$ for $H//c$ approaches the maximum at (3.4 K, 13.8 kOe). The $|\Delta S_M^{ab}(T,H)|$ with $H \perp c$ originates from a field-modulated helicoidal spin-texture. However, the $|\Delta S_M^{c}(T,H)|$ with $H//c$ results from a field-induced canted antiferromagnetic state.

Acknowledgments

This work was supported by the National Key R&D Program of China (Grant Nos. 2017YFA0303201), the National Natural Science Foundation of China (Grant Nos. 11574322, 11874358, U1732276, 11574288, and 11974181), and the Users with Excellence Program of Hefei Science Center CAS (2019HSC-UE010). A proportion of this work was supported by the High Magnetic Field Laboratory of Anhui Province.

ORCID iDs

Jiyu Fan https://orcid.org/0000-0001-6698-6384
Lei Zhang https://orcid.org/0000-0001-5427-6561

References

[1] Rößler U K, Bogdanov A N and Pfleiderer C 2006 *Nature* **442** 797
[2] Yu X, Onose Y, Kanazawa N, Park J, Han J, Matsui Y, Nagaosa N and Tokura Y 2010 *Nature* **465** 901
[3] Yu X, Koshibae W, Tokunaga Y, Shibata K, Taguchi Y, Nagaosa N and Tokura Y 2018 *Nature* **564** 95
[4] Kurumaji T, Nakajima T, Hirschberger M, Kikkawa A, Yamasaki Y, Sagayama H, Nakao H, Taguchi Y, Arima T and Tokura Y 2019 *Science* **365** 914
[5] Zheng F *et al* 2018 *Nat. Nanotechnol.* **13** 45
[6] Leonov A O, Monchesky T L, Romming N, Kubetzka A, Bogdanov A N and Wiesendanger R 2016 *New J. Phys.* **18** 065003
[7] Togawa Y, Koyama T, Takayanagi K, Mori S, Kousaka Y, Akimitsu J, Nishihara S, Inoue K, Ovchinnikov A S and Kishine J 2012 *Phys. Rev. Lett.* **108** 107202
[8] Seki S, Yu X Z, Ishiwata S and Tokura Y 2012 *Science* **336** 198
[9] Mühlbauer S, Binz B, Jonietz F, Pfleiderer C, Rosch A, Neubauer A, Georgii R and Böni P 2009 *Science* **323** 915
[10] Mito M *et al* 2018 *Phys. Rev.* B **97** 024408
[11] Bogdanov A and Hubert A 1994 *J. Magn. Magn. Mater.* **138** 255
[12] Bogdanov A and Hubert A 1999 *J. Magn. Magn. Mater.* **195** 182
[13] Wilson M N, Butenko A B, Bogdanov A N and Monchesky T L 2014 *Phys. Rev.* B **89** 094411
[14] Dzyaloshinski I E 1964 *Sov. Phys.—JETP* **19** 960
[15] Bogdanov A N and Yablonski D A 1989 *Sov. Phys.—JETP* **68** 101
[16] Ninomiya H, Sato T, Inoue K and Ohara S 2018 *Physica* B **536** 654
[17] Aoki R, Togawa Y and Ohara S 2018 *Phys. Rev.* B **97** 214414
[18] Matsumura T, Kita Y, Kubo K, Yoshikawa Y, Michimura S, Inami T, Kousaka Y, Inoue K and Ohara S 2017 *J. Phys. Soc. Japan* **86** 124702
[19] Gladyshevskii R, Cenzual K, Flack H and Parthé E 1993 *Acta Crystallogr.* B **49** 468
[20] Togawa Y, Yusuke Kousaka, Katsuya Inoue and Kishine J 2016 *J. Phys. Soc. Japan* **85** 112001
[21] Tobash P H, Jiang Y, Ronning F, Booth C H, Thompson J D, Scott B L and Bauer E D 2011 *J. Phys.: Condens. Matter* **23** 086002
[22] Yamashita T, Miyazaki R, Aoki Y and Ohara S 2012 *J. Phys. Soc. Japan* **81** 034705
[23] Ohara S, Yamashita T, Mori Y and Sakamoto I 2011 *J. Phys.: Conf. Ser.* **273** 012048
[24] Utsumi Y *et al* 2012 *Phys. Rev.* B **86** 115114
[25] Miyazaki R, Aoki Y, Higashinaka R, Sato H, Yamashita T and Ohara S 2012 *Phys. Rev.* B **86** 155106
[26] Hirayama T, Matsubayashi K, Yamashita T, Ohara S, Munakata K and Uwatoko Y 2012 *J. Phys.: Conf. Ser.* **391** 012020
[27] Shinozaki M, Masaki Y, Aoki R, Togawa Y and Kato Y 2018 *Phys. Rev.* B **97** 214413
[28] Fan J, Xie J, Ying Y, Pi L and Zhang Y 2006 *Solid State Commun.* **138** 299
[29] Jamaluddin S, Manna S, Giri B, Madduri P, Parkin S and Nayak A 2019 *Adv. Funct. Mater.* **29** 1901776
[30] Bocarsly J, Need R, Seshadri R and Wilson S 2018 *Phys. Rev.* B **97** 100404
[31] Dai Y, Liu W, Wang Y, Fan J, Pi L, Zhang L and Zhang Y 2019 *J. Phys.: Condens. Matter* **31** 195803
[32] Liu W, Wang Y, Fan J, Pi L, Ge M, Zhang L and Zhang Y 2019 *Phys. Rev.* B **100** 104403
[33] Pecharsky V and Gscheidner K 1999 *J. Magn. Magn. Mater.* **200** 44
[34] Franco V, Conde A, Romero-Enrique J and Blazquez J 2008 *J. Phys.: Condens. Matter* **20** 285207
[35] Franco V, Blazquez J S and Conde A 2006 *Appl. Phys. Lett.* **89** 222512
[36] Franco V and Conde A 2010 *Int. J. Refrig.* **33** 465
[37] Zhang L, Fan J, Tong W, Ling L, Pi L and Zhang Y 2012 *Physica* B **407** 3543
[38] Ge M, Zhang L, Menzel D, Han H, Jin C, Zhang C, Pi L and Zhang Y 2015 *J. Alloys Compd.* **649** 46